Ergodicity breaking in active run-and-tumble particles in a double-well potential

Urna Basu [1,*], Satya N. Majumdar [2] and Alberto Rosso [2]
[1] *S. N. Bose National Centre for Basic Sciences, Kolkata 700106, India*
[2] *LPTMS, CNRS, Université Paris-Saclay, 91405 Orsay, France*

(Received 15 January 2026; revised 14 April 2026; accepted 6 May 2026; published 18 May 2026)

We investigate the dynamics of a run-and-tumble particle in a double-well potential and demonstrate that, in stark contrast to Brownian particles, active dynamics can lead to strong ergodicity breaking. When the barrier height exceeds a critical threshold, the long-time position distribution depends crucially on the initial condition: If the particle starts within the basin of attraction of one well, it remains trapped there, while if it begins between the two basins, it can reach either well with a finite probability, which we compute exactly via hitting probabilities. Below the critical barrier height, ergodicity is restored and the system converges to a unique stationary distribution, which we derive analytically. Using this result, we also estimate the characteristic barrier-crossing time and show that it violates Kramers-Arrhenius law and displays a divergence near the critical height following a Vogel-Fulcher-Tammann-like form with an anomalous exponent 1/2.

DOI: 10.1103/jysw-w2mb

Active particles—from synthetic Janus colloids to motile cells—display striking behaviors with no counterpart in equilibrium systems [1–4]. Their persistent motion gives rise to qualitatively new phenomena at the collective level, such as flocking [5], motility-induced phase separation [6], and confinement-induced effects [7,8], as well as at the single-particle level, including anomalous position fluctuations [9–15] and unusual first passage properties [16–19]. In the absence of thermal fluctuations, a single particle in an external confining potential shows a non-Boltzmann stationary state, being typically bounded in a finite region, with its position most likely to be a finite distance away from the minimum of the potential in the limit of strong activity [20–24]. This raises an important question about the position fluctuations of active particles in landscapes with multiple minima separated by finite barriers, which is virtually unexplored.

A related question is how the escape time of a particle across a barrier is affected by the presence of activity. For passive Brownian particles, the typical time to cross a barrier of height ΔV is given by the Kramers' law $\tau \sim \exp(\beta \Delta V)$, where β is the inverse temperature [25,26]. However, how much of this universal feature remains valid in the presence of activity is an open question. This question has been investigated in the presence of single or multiple barriers, in the limits of strong and weak activities [27–31]. Recently, the transition rate between the two wells for an active particle in a double-well potential has also been measured experimentally [32], which shows the existence

*Contact author: urna@bose.res.in

Published by the American Physical Society under the terms of the Creative Commons Attribution 4.0 International license. Further distribution of this work must maintain attribution to the author(s) and the published article's title, journal citation, and DOI.

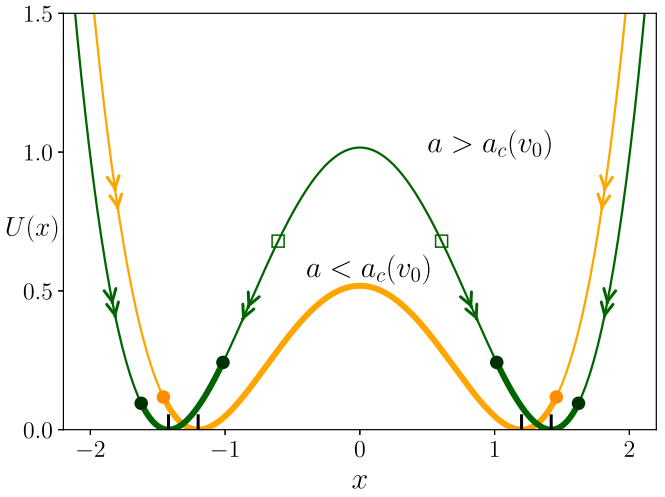


FIG. 1. Schematic representation of the double-well potential for $a < a_c$ (light orange curve) and $a > a_c$ (dark green curve). The thick sections of the curves indicate the support of the stationary position distribution in the respective cases, and the arrows indicate the direction of the net force on the RTP. For $a > a_c$, the empty squares indicate the points $x = \pm\ell_1$ and the filled discs indicate $x = \pm\ell_2$ and $x = \pm\ell_3$.

of an optimum activity that maximizes the transition rate. However, most of these works focus on the finite-temperature scenario, where thermal noise already allows the particle to cross the barrier. How the pure active nature of the dynamics, without additional thermal fluctuations, affects the barrier-crossing time, however, remains elusive and is one of the main focuses of this work.

In this article, we consider the simplest nontrivial setting, namely, motion of an active run-and-tumble particle (RTP) in a double-well potential in one dimension. We consider a symmetric double-well potential $U(x) = \frac{1}{4}(x^2 - a^2)^2$, which has two minima at $x = \pm a$ separated by a barrier of height $U(0) = a^4/4$ (see Fig. 1). Such potentials are paradigmatic setup for investigation of barrier-crossing phenomenon. For a passive Brownian particle initially localized in one well, the probability of crossing to the other well is governed by the Kramers/Arrhenius law, which leads to a finite mean escape time. Consequently, the particle eventually explores both wells and relaxes to a unique stationary Boltzmann distribution, a result that holds irrespective of the precise shape of the potential. In this work, we show that the picture is fundamentally different for an active particle, both for position fluctuations and for barrier-crossing time. We begin by analyzing the stationary position distribution of an RTP in a double-well potential.

The position $x(t)$ of an RTP in the double-well potential $U(x)$ evolves following the Langevin equation,

$$\dot{x}(t) = f(x) + v_0\sigma(t), \tag{1}$$

where

$$f(x) \equiv -U'(x) = -x(x^2 - a^2) \tag{2}$$

is the force on the particle from the potential. In the absence of any external force, the particle moves with a constant speed v_0 along its internal orientation σ, which alternates between ± 1 with a rate γ.

The bounded nature of the active dichotomous noise $\sigma(t)$ implies that the RTP cannot dynamically access the regions where $|f(x)| > v_0$. Thus, the turning points, where $f(x) = \pm v_0$, act as effective walls, confining the particles in a finite region. For the double-well potential, the force $f(x)$ is a nonmonotonic and odd function of x, with extrema at $x = \pm m$, where $m = a/\sqrt{3}$ (see Fig. 2). Clearly, if $|f(m)| = 2a^3/3\sqrt{3} < v_0$, there is a unique solution for $f(x) = v_0$. Thus, for

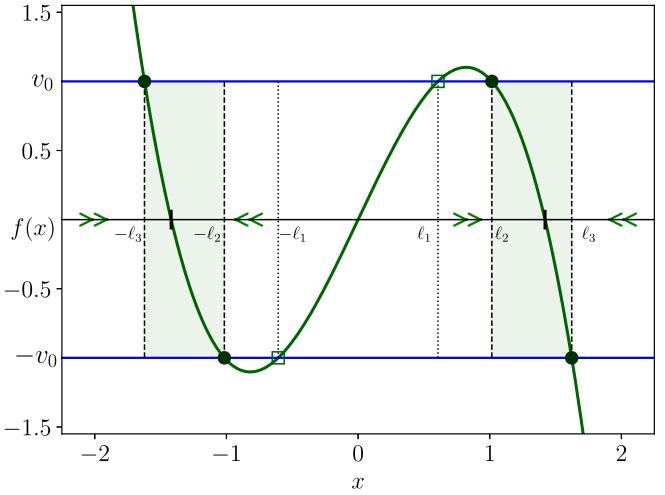


FIG. 2. Schematic representation of the fixed points of the force $f(x)$ for $a > a_c$. Here, we have taken $a = 1.42$ and $v_0 = 1$ so that $a_c \simeq 1.3747$. The shaded green regions indicate the supports of the stationary distribution. The dotted lines indicate the boundaries of the basins of attractions of the two wells. The arrows along the x axis indicate the direction of the force on the particle in the respective regions.

$a < a_c$, where

$$a_c = \left(\frac{3\sqrt{3}\, v_0}{2}\right)^{1/3}, \tag{3}$$

there are only two turning points $x = \pm\ell(a)$ and the particle will be confined in the region $-\ell(a) \leqslant x \leqslant \ell(a)$. The corresponding stationary distribution is ergodic and can be obtained using the generic result derived in Refs. [20,33] for arbitrary confining potentials,

$$P_{\rm st}(x) = \frac{\mathcal{N}}{v_0^2 - f^2(x)} \exp\left[2\gamma \int_0^x \frac{{\rm d}u\, f(u)}{v_0^2 - f^2(u)}\right], \tag{4}$$

where $\mathcal{N}$ is the normalization constant, given by

$$\mathcal{N}^{-1} = \int_{-\ell}^{\ell} \frac{{\rm d}x}{v_0^2 - f^2(x)} \exp\left[2\gamma \int_0^x \frac{{\rm d}u\, f(u)}{v_0^2 - f^2(u)}\right]. \tag{5}$$

The scenario becomes much more complex and interesting for $a > a_c$, where the equation $f(x) = v_0$ has three real solutions. Consequently, there are six turning points, denoted by $\pm\ell_1$, $\pm\ell_2$, and $\pm\ell_3$; for notational convenience, we assume $\ell_3 > \ell_2 > \ell_1 > 0$. These turning points divide the phase space (the real line) into seven distinct regimes, as illustrated in Fig. 2. The splitting of phase space into disconnected regions results in a position distribution that is inherently nonergodic. In the following, we first investigate the position fluctuations in the nonergodic regime $a > a_c$.

I. NONERGODIC REGIME

To understand the behavior of the stationary position distribution for $a > a_c$, it is useful to consider the Langevin equation (1) and investigate the net force acting on the particle in the different regions. For $x > \ell_3$ and $\ell_1 \leqslant x \leqslant \ell_2$, $|f(x)| > v_0$ and the particle feels an attractive force toward the right well, irrespective of its internal orientation (see Fig. 2). Furthermore, once the particle enters the region $\ell_2 \leqslant x \leqslant \ell_3$, it cannot escape. Thus, the region $x > \ell_1$ forms the "basin of attraction" for the right well—If the initial position of the particle $x_0 > \ell_1$, the particle eventually falls in the right

well and gets trapped in the region $\ell_2 \leqslant x \leqslant \ell_3$. Similarly, if initially the particle is in the region $x < -\ell_1$, it eventually falls in the left well and remains trapped in the region $-\ell_3 \leqslant x \leqslant -\ell_2$. However, if the initial position of the particle is in the intermediate domain, i.e., $|x_0| < \ell_1$, then the direction of the net force on the particle depends on its orientation $\sigma(t)$, and it can move in both directions until getting trapped in one of the wells. Thus, for $a > a_c$, i.e., when the barrier height is larger than a critical value, the position distribution of the RTP depends on its initial position, leading to a breakdown of ergodicity in the stationary state. Such ergodicity breaking is a direct consequence of the active nature of the particle and is absent in passive (Brownian) systems. In the following, we characterize this nonergodic position distribution, which constitutes one of the central results of this work.

First, we consider the case $x_0 > \ell_1$, i.e., when the particle starts within the basin of attraction of the right well. As mentioned above, in this case, the particle is confined in the region $\ell_2 \leqslant x \leqslant \ell_3$ in the steady state. The corresponding stationary distribution can be obtained using Eq. (4),

$$P_R(x) = \frac{\mathcal{N}_R}{v_0^2 - f^2(x)} \exp\left[2\gamma \int_a^x \frac{\mathrm{d}u\, f(u)}{v_0^2 - f^2(u)}\right]. \tag{6}$$

Note that this distribution is supported in the region $\ell_2 \leqslant x \leqslant \ell_3$ and the normalization constant is given by

$$\mathcal{N}_R^{-1} = \int_{\ell_2}^{\ell_3} \frac{\mathrm{d}x}{v_0^2 - f^2(x)} \exp\left[2\gamma \int_a^x \frac{\mathrm{d}u\, f(u)}{v_0^2 - f^2(u)}\right]. \tag{7}$$

Next, we consider the case $x_0 < -\ell_1$, i.e., when the particle starts within the basin of attraction of the left well. The symmetry of the potential implies that the stationary distribution of the RTP in this case is given by

$$P_L(x) = P_R(-x). \tag{8}$$

Obviously, $P_L(x)$ is supported in the region $-\ell_3 \leqslant x \leqslant -\ell_2$. Figure 3 shows plots of the position distribution of the RTP when it is trapped in one of the wells.

The most nontrivial situation emerges when the initial position x_0 falls outside the basins of attraction of both the wells, i.e., in the intermediate domain $|x_0| < \ell_1$. In this case, the RTP moves randomly until it reaches one of the basins and then gets trapped in the corresponding well. Thus, the position distribution depends explicitly on the initial position when it lies in the intermediate region between the basins of attraction of the two wells. In this case, we can define the position distribution $P(x; x_0)$ averaged over all possible realizations with a fixed initial position x_0. To compute it, we need to find the probability of the RTP exiting the region $-\ell_1 \leqslant x \leqslant \ell_1$ through the right or left boundary. This is the classic "hitting probability," sometimes also referred to as "splitting probability"—For a one-dimensional stochastic process x_t in an interval, the hitting probability quantifies the likelihood that starting at a fixed position x_0, the process reaches one boundary of the interval before the other. For ordinary Brownian motion, this probability is known, both in free space [34] and in presence of an arbitrary potential [35]. The hitting probability for an RTP particle in an arbitrary potential has also been computed very recently [36], which we rederive in Appendix A using our notations. Our results are summarized as follows.

Let $Q_\sigma(x_0)$ denote the probability that, starting from x_0 with internal orientation σ, the RTP hits the right boundary $x = \ell_1$ before hitting the left boundary $x = -\ell_1$. It can be shown that $Q_\sigma(x_0)$ satisfies the backward Fokker-Planck equation

$$[f(x_0) + \sigma v_0]\frac{dQ_\sigma}{dx_0} + \gamma[Q_{-\sigma}(x_0) - Q_\sigma(x_0)] = 0, \tag{9}$$

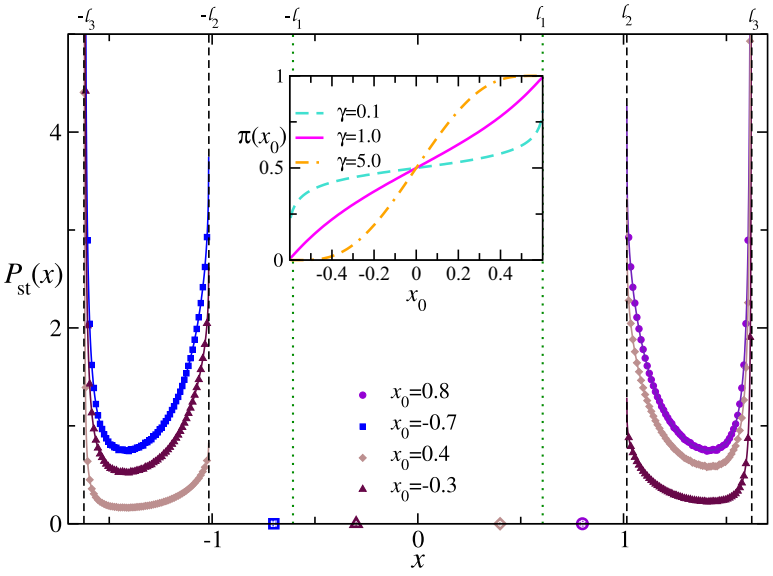


FIG. 3. Nonergodic phase: Plot of $P_{st}(x)$ for $a = 1.42 > a_c$ and different values of initial position x_0, for $\gamma = 1$. The solid lines correspond to the analytical prediction [Eq. (13)] and symbols to numerical simulations. The dotted vertical lines indicate $x = \pm\ell_1$, whereas the dashed vertical lines indicate $x = \pm\ell_2$ and $x = \pm\ell_3$. Here, we have taken $v_0 = 1$ so that $a_c \approx 1.3747$ and $\ell_1 \approx 0.6067$, $\ell_2 \approx 1.0159$, and $\ell_3 \approx 1.6226$. The symbols on the x axis mark the values of x_0 corresponding to the four curves. The inset shows the plot of the hitting probability $\pi(x_0)$ vs x_0 in the regime $-\ell_1 \leqslant x_0 \leqslant x_0$ for different values of γ. The values of a and v_0 used are same as in the main plot.

with the boundary conditions $Q_+(\ell_1) = 1$ and $Q_-(-\ell_1) = 0$ (see Appendix A for details). This set of coupled first-order differential equations can be solved exactly to obtain

$$Q_+(x_0) = \frac{1}{1+\gamma G}\left[1 + \gamma \int_{-\ell_1}^{x_0} \frac{dy}{v_0 + f(y)} e^{-2\gamma \int_{-\ell_1}^{y} \frac{du f(u)}{v_0^2 - f^2(u)}}\right],$$

$$Q_-(x_0) = \frac{\gamma}{1+\gamma G} \int_{-\ell_1}^{x_0} \frac{dy}{v_0 - f(y)} e^{-2\gamma \int_{-\ell_1}^{y} \frac{du f(u)}{v_0^2 - f^2(u)}}, \tag{10}$$

where

$$G = \int_{-\ell_1}^{\ell_1} \frac{dy}{v_0 + f(y)} \exp\left[-2\gamma \int_{-\ell_1}^{y} \frac{du\, f(u)}{v_0^2 - f^2(u)}\right]. \tag{11}$$

Thus, the probability that the RTP, starting from the intermediate region $-\ell_1 \leqslant x_0 \leqslant \ell_1$, gets trapped in the right well is given by

$$\pi(x_0) = \tfrac{1}{2}[Q_+(x_0) + Q_-(x_0)], \tag{12}$$

where we have assumed that the initial orientation $\sigma = \pm 1$, with equal probability 1/2. Inset of Fig. 3 shows plot of $\pi(x_0)$ as a function of x_0. Clearly, it increases monotonically indicating the particle preferably exits the interval via the closer boundary. However, the nonlinear nature is a signature of the active nature of the motion.

Using the above results, we arrive at the average position distribution in the long-time limit,

$$P(x; x_0) = \pi(x_0) P_{st}^R(x) + [1 - \pi(x_0)] P_{st}^L(x). \tag{13}$$

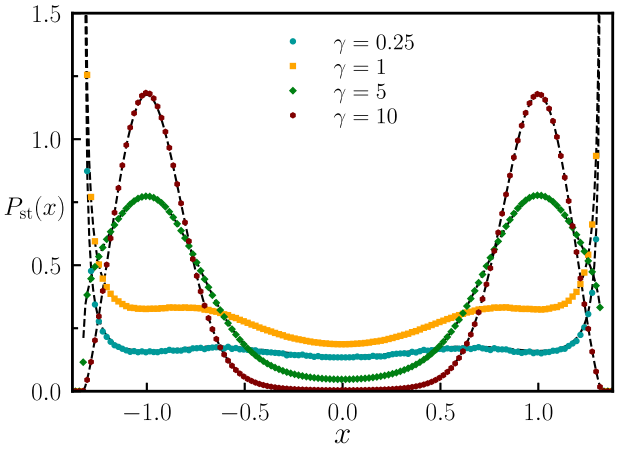


FIG. 4. Position distribution in the ergodic regime: Plot of $P_{\rm st}(x)$ vs x for $a = 1$ for different values of γ. The symbols correspond to the data obtained from numerical simulations, while the dashed black lines correspond to the analytical prediction [Eq. (4)].

Figure 3 compares the above predicted distribution with the same obtained from numerical simulations for two different values of x_0, which show excellent agreement. Note that, in this case, the stationary distribution cannot be obtained by time averaging and one has to average over independent trajectories to measure the distribution correctly. This is an example of strong nonergodicity, which has also been observed in the context of RTP in a periodic potential [37]. Ergodicity breaking in a weaker sense has been also observed in the context of anomalous diffusion processes [38–40].

II. ERGODIC REGIME

It is also useful to look at the shape of the stationary position distribution in the ergodic phase, i.e., for $a < a_c$. In the ergodic phase, the stationary distribution is unique and is given by Eqs. (4) and (5). As mentioned before, in this case, the distribution is supported in the regime $-\ell \leqslant x \leqslant \ell$. Although it is hard to obtain a closed form for the position distribution, it can be estimated with arbitrary accuracy by performing the integral numerically. Figure 4 illustrates how the shape of $P_{\rm st}(x)$ changes with the flip rate γ—The position distribution undergoes a shape transition as γ is varied. Similar to an RTP in a harmonic potential [20], the distribution is strongly peaked near the boundaries $x = \pm\ell$ for small γ. For large γ, the particle effectively behaves like a Brownian one, leading to a Boltzmann-like distribution with two peaks around $x = \pm a$.

III. BARRIER CROSSING

The double-well setup provides an ideal playground to study the barrier-crossing phenomenon for active particles. The most important quantity of interest in this regard is the characteristic timescale associated with crossing the barrier between the two wells. In the nonergodic phase, the particle remains localized in one of the wells indefinitely, and therefore, the barrier-crossing time diverges. In contrast, in the ergodic phase $a < a_c$, the RTP is able to cross the barrier and the corresponding time remains finite. A convenient measure of this timescale can be constructed from the weight of the stationary distribution at the location of the barrier. More precisely, we define

$$\tau = 1/[v_0 P_{\rm st}(0)] = v_0 \mathcal{N}^{-1}, \tag{14}$$

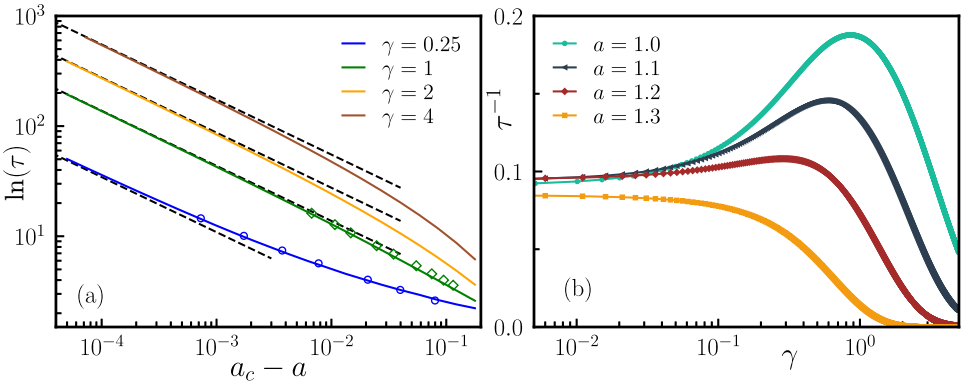


FIG. 5. Barrier-crossing time in the ergodic phase: (a) Plot of $\ln(\tau)$ vs $a_c - a$ in the log-log scale for different values of flip rate γ. The solid lines indicate the data obtained from numerically integrating Eq. (5), while the dashed black lines indicate the near-critical $(a_c - a)^{-1/2}$ behavior predicted in Eq. (16). The symbols indicate the characteristic dwelling time measured from simulations. (b) Plot of escape rate as a function of γ for different values of a, obtained from numerically integrating Eq. (5) and using Eq. (14).

where $\mathcal{N}$ is given in Eqs. (4) and (5). This, in turn, enables an analytical study of the barrier-crossing time, allowing us to investigate how τ scales as the barrier height approaches the critical threshold a_c.

To analyze the behavior of $\mathcal{N}$, let us first note that, for $a = a_c$, we have $|f(x)| = v_0$ at $x = \pm m$. Consequently, the integrand in Eq. (5) diverges as $a \to a_c$, and for small $\epsilon = a_c - a$, the dominant contribution to the integral comes from near $x = m$. This observation allows us to compute the asymptotic behavior of $P_{\rm st}(0)$ for small ϵ, which finally leads to (see Appendix B for the details)

$$\tau \propto \frac{1}{\sqrt{v_0(a_c - a)}} \exp\left[\frac{\pi\gamma}{3^{3/4}\sqrt{v_0(a_c - a)}}\right]. \tag{15}$$

Consequently, as $a \to a_c$, the leading asymptotic behavior of the barrier-crossing time becomes

$$\ln \tau \approx \frac{\pi\gamma}{3^{3/4}}[v_0(a_c - a)]^{-1/2}. \tag{16}$$

Figure 5(a) illustrates this algebraic divergence of $\ln \tau$.

Another measure of the barrier-crossing time is provided by the decay timescale of the dwelling-time distribution of the RTP within a well, which typically exhibits an exponential tail. This characteristic decay time, measured from numerical simulations, shows excellent agreement with the analytically predicted τ, as illustrated in Fig. 5(a).

The behavior of the barrier-crossing time, given in Eq. (16), constitutes the second key finding of this work. It shows that for an RTP, the barrier-crossing phenomenon is fundamentally different from that for the passive particles—Without the help of thermal noise, the active particle is able to cross a barrier only when its height is smaller than the threshold value, which depends on its self-propulsion velocity. Moreover, the typical time required to cross the barrier shows a super-Arrhenius growth, diverging as the height approaches the threshold value. The divergence resembles a Vogel-Fulcher-Tammann law seen in glassy systems [41], albeit with an anomalous exponent 1/2 instead of the standard exponent 1.

It should be emphasized that the crucial element underlying this strong ergodicity breaking and divergence of barrier-crossing time for an RTP is the bounded nature of the dichotomous active noise $\sigma(t)$. In contrast, the active Ornstein-Uhlenbeck process (AOUP) [42], driven by Gaussian noise, is not expected to exhibit strong ergodicity breaking. Indeed, for an AOUP in a double-well

potential, the barrier-crossing time displays an Arrhenius-like dependence with an effective barrier height in the weak-noise limit [43].

A recent experiment on active Brownian particles in a double-well potential [32] reported that the transition rate between the wells, equivalent to τ^{-1}, exhibits a pronounced nonmonotonic dependence on the rotational diffusion constant, reaching a maximum at an optimal value. In this context, it is worthwhile to investigate how τ depends on the flip rate γ, especially for $a \ll a_c$, where Eq. (16) is not expected to hold. In this regime, τ can be obtained by numerically evaluating the integral in Eq. (5), which reproduces the experimentally observed nonmonotonic behavior. As shown in Fig. 5(b), the escape rate τ^{-1} varies nonmonotonically with γ, attaining a maximum at an intermediate flip rate that shifts to smaller values as $a \to a_c$. The physical origin of the nonmonotonicity can be understood as follows: For small γ, the particle is most likely to be near $\pm\ell(a)$, i.e., away from the barrier, which makes it harder for it to cross the barrier, which leads to a large value of τ. As γ is increased, the particle has a larger chance to be near the barrier (cf. the $\gamma = 1$ curve in Fig. 4), thus reducing the τ. For very large γ, the RTP typically behaves like a passive particle, with the position distribution being peaked at $\pm a$; i.e., it goes farther away from the barrier, thus increasing τ again.

IV. CONCLUSIONS

We have shown that a run-and-tumble particle in a double-well potential exhibits a sharp ergodicity-breaking transition controlled by the barrier height. Above a critical threshold, the dynamics partition the phase space into disconnected regions, leading to stationary distributions that depend on the initial condition; below it, ergodicity is restored and the unique stationary state can be obtained exactly. Our analysis further shows that an active particle behaves in a fundamentally different manner from its passive counterpart in barrier-crossing processes, with a strong violation of the Arrhenius law. Our results are easily generalized for multiwell situations and can possibly be verified experimentally using a setup similar to Ref. [32]. It would be interesting to see whether the ergodicity-breaking transition found here also shows up for interacting many-particle systems. A promising recent result in that direction was found in Ref. [44], where similar breaking of ergodicity was observed in a one-dimensional system of RTPs interacting via pairwise double-well potential.

ACKNOWLEDGMENTS

The authors thank Gregory Schehr for useful discussions. U.B. acknowledges the support from the Anusandhan National Research Foundation (ANRF), India, under a MATRICS Grant (No. MTR/2023/000392). S.N.M. acknowledges support from ANR Grant No. ANR-23-CE30-0020-01 EDIPS.

DATA AVAILABILITY

The data that support the findings of this article are not publicly available. The data are available from the authors upon reasonable request.

APPENDIX A: COMPUTATION OF THE HITTING PROBABILITY

In this Appendix, we outline the steps leading to the explicit computation of the hitting probability $\pi(x_0)$. Let $Q_\sigma(x_0)$ denote the probability that, starting from some initial position x_0 with orientation σ, the RTP exits the intermediate region through the right boundary $x = \ell_1$. To compute this probability, it is most convenient to adopt the backward Fokker-Planck equation approach. Considering the possible trajectories over the interval $[0, \Delta t]$, we can write the backward FP equation

$$Q_\sigma(x_0) = (1 - \gamma\Delta t)Q_\sigma(x_0 + (f(x_0) + v_0\sigma)\Delta t) + \gamma\Delta t Q_{-\sigma}(x_0), \tag{A1}$$

where the first term on the right-hand side corresponds to the contribution from the trajectories with no flip during this interval and the second term denotes the contribution from the trajectories with a flip. Expanding $Q_\sigma(x)$ in Taylor's series and taking $\Delta t \to 0$ limit, we get two coupled equations for $\sigma = \pm 1$:

$$[f(x_0) + v_0]\frac{dQ_+}{dx_0} - \gamma(Q_+(x_0) - Q_-(x_0)) = 0,$$
$$[f(x_0) - v_0]\frac{dQ_-}{dx_0} + \gamma(Q_+(x_0) - Q_-(x_0)) = 0. \tag{A2}$$

To solve these equations, we need to determine the boundary conditions satisfied by $Q_\sigma(x_0)$. To this end, let us first consider the case where the particle starts from $x = -\ell_1$, with $\sigma = -1$. In this case, the particle is expected to immediately exit the intermediate region through the left boundary. Similarly, if the particle starts at $x_0 = \ell_1$ with $\sigma = 1$, it is expected to exit through the right boundary. Thus, $Q_\pm(x_0)$ must satisfy the boundary conditions

$$Q_+(\ell_1) = 1 \quad \text{and} \quad Q_-(-\ell_1) = 0. \tag{A3}$$

To solve Eq. (A2), it is convenient to recast these in terms of $Q(x_0) = Q_+(x_0) + Q_-(x_0)$ and $F(x_0) = Q_+(x_0) - Q_-(x_0)$ as

$$f(x_0)\frac{dQ}{dx_0} + v_0\frac{dF}{dx_0} = 0,$$
$$f(x_0)\frac{dF}{dx_0} + v_0\frac{dQ}{dx_0} = 2\gamma F(x_0). \tag{A4}$$

Multiplying the second equation by $f(x_0)$ and substituting the first equation, we have a first-order differential equation for $F(x_0)$:

$$\left[f(x_0)^2 - v_0^2\right]\frac{dF}{dx_0} - 2\gamma f(x_0)F(x_0) = 0. \tag{A5}$$

This can be solved immediately to get

$$F(x_0) = A\exp\left[-2\gamma\int_{-\ell}^{x_0}\frac{du f(u)}{v_0^2 - f(u)^2}\right], \tag{A6}$$

where A is an arbitrary constant. Using this solution in Eq. (A4), we obtain $Q_\pm(x_0)$,

$$Q_+(x_0) = \gamma\int_{-\ell}^{x_0}\frac{dy}{v_0 + f(y)}F(y) + B_1,$$
$$Q_-(x_0) = \gamma\int_{-\ell}^{x_0}\frac{dy}{v_0 - f(y)}F(y) + B_2, \tag{A7}$$

where B_1, B_2 are arbitrary constants. It is easy to see that B_1, B_2, and A must be related by $B_1 - B - 2 = A$, since $F(-\ell_1) = Q_+(-\ell_1) - Q_-(-\ell_1)$. Using this relation and the boundary condition (A3), we can determine $Q_\pm(x_0)$ explicitly, which are quoted in Eq. (10).

APPENDIX B: COMPUTATION OF THE BARRIER-CROSSING TIMESCALE

In this Appendix, we provide the detailed steps involved in computing the barrier-crossing timescale τ, starting from Eq. (14). From the definition of $\mathcal{N}$ in Eq. (5), we can write

$$\tau = 2v_0\int_0^\ell\frac{dx}{v_0^2 - f(x)^2}\exp\left[2\gamma\int_0^x\frac{du f(u)}{v_0^2 - f(x)^2}\right]. \tag{B1}$$

Our goal is to investigate the behavior of τ as $\epsilon = a_c - a \to 0$. To this end, we first note that, for small ϵ, the dominant contribution to the above integral comes from near the maximum of $f(x)$,

i.e, when x is close to $m = a/\sqrt{3}$. Consequently, it is convenient to separate the integral into three regions: $0 \leqslant x \leqslant m - \Delta$, $m - \Delta \leqslant x \leqslant m + \Delta$, and $m + \Delta \leqslant x \leqslant \ell$, where $\Delta/m \lesssim 1$. For small $\epsilon = a_c - a$, the dominating contribution comes from the middle region, and we can write

$$\tau \simeq 2v_0 \int_{m-\Delta}^{m+\Delta} \frac{dx}{v_0^2 - f(x)^2} \exp\left[2\gamma \int_0^x \frac{duf(u)}{v_0^2 - f(x)^2}\right] + O(1). \tag{B2}$$

Let us first consider the behavior of the integral inside the exponential, namely,

$$G(x) = 2\gamma \int_0^x \frac{duf(u)}{v_0^2 - f(u)^2}. \tag{B3}$$

Once again, for small values of ϵ, this integral is dominated by the contribution from near $u = m$, and we can write

$$G(x) = 2\gamma \int_{m-\Delta}^x \frac{duf(u)}{v_0^2 - f(u)^2} + O(1). \tag{B4}$$

Now, close to $u = m$, $f(u)$ has a quadratic form:

$$f(u) \simeq f(m) + \frac{1}{2}(u - m)^2 f''(m) = v_0\left(\frac{a}{a_c}\right)^3 - \sqrt{3}a(u - m)^2. \tag{B5}$$

The above quadratic form leads to, to the second order in $(u - m)$,

$$v_0^2 - f(u)^2 \simeq v_0^2\left[1 - \left(\frac{a}{a_c}\right)^6\right] + 2\sqrt{3}v_0\frac{a^4}{{a_c}^3}(u - m)^2. \tag{B6}$$

Using the definition of a_c [see Eq. (3)], this can be simplified to

$$v_0^2 - f(u)^2 \simeq \tfrac{4}{3}a^4[\delta^2 + (u - m)^2], \tag{B7}$$

where we have defined

$$\delta^2 = \frac{3v_0^2}{4a^4}\left[1 - \left(\frac{a}{a_c}\right)^6\right]. \tag{B8}$$

Now, using Taylor's expansion for small $\epsilon = a_c - a$, we have

$$\delta^2 = \tfrac{2}{3}a_c\epsilon + O(\epsilon^2). \tag{B9}$$

Next, substituting Eq. (B7) into Eq. (B4), we get, to the leading order in ϵ,

$$G(x) \simeq \frac{3\gamma v_0}{2a_c^4} \int_{m-\Delta}^x \frac{du}{\delta^2 + (u - m)^2}, \tag{B10}$$

where we have used the fact that $f(m) = v_0$ at $a = a_c$. This integral can be performed to obtain

$$G(x) \simeq \frac{\gamma}{\sqrt{3}a_c\delta}\left[\tan^{-1}\frac{x - m}{\delta} + \tan^{-1}\frac{\Delta}{\delta}\right]. \tag{B11}$$

For $\epsilon \to 0$, i.e., $\delta \to 0$, and $\Delta \sim O(1)$, $\tan^{-1}(\Delta/\delta) \to \pi/2$, while $\tan^{-1}((x - m)/\delta) \to \mathrm{sgn}(x - m)\pi/2$. Thus,

$$G(x) = \frac{\gamma\pi}{\sqrt{3}a_c\delta}\Theta(x - m) + O(1), \tag{B12}$$

where $\Theta(z)$ denotes the Heaviside theta funtion. Substituting the above expression in Eq. (B2), we get

$$\tau = 2v_0A_1 \exp\left(\frac{\pi\gamma}{\sqrt{3}a_c\delta}\right) \int_m^{m+\Delta} \frac{dx}{v_0^2 - f^2(x)}, \tag{B13}$$

where A_1 is a constant that does not depend on ϵ. Using Eq. (B7) for the integrand, we get

$$\tau = \frac{3v_0 A_1}{2a_c^4 \delta} \exp\left(\frac{\pi\gamma}{\sqrt{3}a_c\delta}\right) \tan^{-1}\frac{\Delta}{\delta}. \tag{B14}$$

In the limit $\delta \to 0$, $\tan^{-1}\frac{\Delta}{\delta} \to \pi/2$. Using Eq. (3), the above equation further simplifies to

$$\tau = A_1 \frac{\pi}{2\sqrt{3}a_c\delta} \exp\left(\frac{\pi\gamma}{\sqrt{3}a_c\delta}\right). \tag{B15}$$

Finally, the behavior of the escape timescale near $a = a_c^-$ can be obtained using Eq. (B9),

$$\tau = \frac{A}{\sqrt{v_0(a_c - a)}} \exp\left[\frac{\pi\gamma}{3^{3/4}\sqrt{v_0(a_c - a)}}\right], \tag{B16}$$

where A is an undetermined factor, possibly depending on γ, a, and v_0. This is quoted in Eqs. (15) and (16).

APPENDIX C: NUMERICAL DETAILS

We numerically simulate the Langevin dynamics [Eq. (1)] using Euler discretization scheme with $dt = 10^{-3}$. We have typically used 10^5–10^7 realizations to measure the position distribution shown in Figs. 3 and 4. To estimate the escape time, we measure the distribution $P(\tau_d)$ of the dwelling time τ_d, which is defined as the time the RTP spends in a well until it crosses the barrier at $x = 0$ for the first time. The characteristic time estimated from the exponential tail of this distribution is shown in Fig. 5 as symbols.

[1] P. Romanczuk, M. Bär, W. Ebeling, B. Lindner, and L. Schimansky-Geier, Active Brownian particles, Eur. Phys. J. Spec. Top. **202**, 1 (2012).

[2] C. Bechinger, R. Di Leonardo, H. Löwen, C. Reichhardt, G. Volpe, and G. Volpe, Active particles in complex and crowded environments, Rev. Mod. Phys. **88**, 045006 (2016).

[3] J. O'Byrne, Y. Kafri, J. Tailleur, and F. van Wijland, Time irreversibility in active matter, from micro to macro, Nat. Rev. Phys. **4**, 167 (2022).

[4] É. Fodor and M. C. Marchetti, The statistical physics of active matter: From self-catalytic colloids to living cells, Physica A **504**, 106 (2018).

[5] A. Cavagna and I. Giardina, Bird flocks as condensed matter, Annu. Rev. Condens. Matter Phys. **5**, 183 (2014).

[6] M. E. Cates and J. Tailleur, Motility-induced phase separation, Annu. Rev. Condens. Matter Phys. **6**, 219 (2015).

[7] L. Caprini and U. Marini Bettolo Marconi, Active particles under confinement and effective force generation among surfaces, Soft Matter **14**, 9044 (2018).

[8] L. Caprini, C. Maggi, and U. Marini Bettolo Marconi, Collective effects in confined active Brownian particles, J. Chem. Phys. **154**, 244901 (2021).

[9] U. Basu, S. N. Majumdar, A. Rosso, and G. Schehr, Active Brownian motion in two dimensions, Phys. Rev. E **98**, 062121 (2018).

[10] I. Santra, U. Basu, and S. Sabhapandit, Active Brownian motion with directional reversals, Phys. Rev. E **104**, L012601 (2021).

[11] K. Malakar, V. Jemseena, A. Kundu, K. Vijay Kumar, S. Sabhapandit, S. N. Majumdar, S. Redner, and A. Dhar, Steady state, relaxation and first-passage properties of a run-and-tumble particle in one-dimension, J. Stat. Mech. (2018) 043215.

[12] G. Gradenigo and S. N. Majumdar, A first-order dynamical transition in the displacement distribution of a driven run-and-tumble particle, J. Stat. Mech. (2019) 053206.

[13] F. Mori, G. Gradenigo, and S. N. Majumdar, First-order condensation transition in the position distribution of a run-and-tumble particle in one dimension, J. Stat. Mech. (2021) 103208.
[14] N. R. Smith and O. Farago, Nonequilibrium steady state for harmonically confined active particles, Phys. Rev. E **106**, 054118 (2022).
[15] N. R. Smith, Nonequilibrium steady state of trapped active particles, Phys. Rev. E **108**, L022602 (2023).
[16] F. Mori, P. Le Doussal, S. N. Majumdar, and G. Schehr, Universal survival probability for a d-dimensional run-and-tumble particle, Phys. Rev. Lett. **124**, 090603 (2020).
[17] F. Mori, P. Le Doussal, S. N. Majumdar, and G. Schehr, Universal properties of a run-and-tumble particle in arbitrary dimension, Phys. Rev. E **102**, 042133 (2020).
[18] S. K. Nath and S. Sabhapandit, Survival probability and position distribution of a run and tumble particle in $U(x) = \alpha|x|$ potential with an absorbing boundary J. Stat. Mech. (2024) 093205.
[19] M. Guéneau, S. N. Majumdar, and G. Schehr, Run-and-tumble particle in one-dimensional potentials: Mean first-passage time and applications, Phys. Rev. E **111**, 014144 (2025).
[20] A. Dhar, A. Kundu, S. N. Majumdar, S. Sabhapandit, and G. Schehr, Run-and-tumble particle in one-dimensional confining potentials: Steady-state, relaxation, and first-passage properties, Phys. Rev. E **99**, 032132 (2019).
[21] U. Basu, S. N. Majumdar, A. Rosso, and G. Schehr, Long-time position distribution of an active Brownian particle in two dimensions, Phys. Rev. E **100**, 062116 (2019).
[22] I. Santra, U. Basu, and S. Sabhapandit, Direction reversing active Brownian particle in a harmonic potential, Soft Matter **17**, 10108 (2021).
[23] D. Chaudhuri and A. Dhar, Active Brownian particle in harmonic trap: Exact computation of moments, and re-entrant transition, J. Stat. Mech. (2021) 013207.
[24] N. R. Smith, P. Le Doussal, S. N. Majumdar, and G. Schehr, Exact position distribution of a harmonically confined run-and-tumble particle in two dimensions, Phys. Rev. E **106**, 054133 (2022).
[25] H. A. Kramers, Brownian motion in a field of force and the diffusion model of chemical reactions, Physica **7**, 284 (1940).
[26] L. Rondin, J. Gieseler, F. Ricci, R. Quidant, C. Dellago, and L. Novotny, Direct measurement of Kramers turnover with a levitated nanoparticle, Nat. Nanotechnol. **12**, 1130 (2017).
[27] A. Sharma, R. Wittmann, and J. M. Brader, Escape rate of active particles in the effective equilibrium approach, Phys. Rev. E **95**, 012115 (2017).
[28] A. Geiseler, P. Hänggi, and G. Schmid, Kramers escape of a self-propelled particle, Eur. Phys. J. B **89**, 175 (2016).
[29] E. Woillez, Y. Zhao, Y. Kafri, V. Lecomte, and J. Tailleur, Activated escape of a self-propelled particle from a metastable state, Phys. Rev. Lett. **122**, 258001 (2019).
[30] L. Caprini, U. Marini Bettolo Marconi, A. Puglisi, and A. Vulpiani, Active escape dynamics: The effect of persistence on barrier crossing, J. Chem. Phys. **150**, 024902 (2019).
[31] D. Wexler, N. Gov, K. Ø. Rasmussen, and G. Bel, Dynamics and escape of active particles in a harmonic trap, Phys. Rev. Res. **2**, 013003 (2020).
[32] A. Militaru, M. Innerbichler, M. Frimmer, F. Tebbenjohanns, L. Novotny, and C. Dellago, Escape dynamics of active particles in multistable potentials, Nat. Commun. **12**, 2446 (2021).
[33] A. P. Solon, Y. Fily, A. Baskaran, M. E. Cates, Y. Kafri, M. Kardar, and J. Tailleur, Pressure is not a state function for generic active fluids, Nat. Phys. **11**, 673 (2015).
[34] S. Redner, *A Guide to First-Passage Processes* (Cambridge University Press, Cambridge, UK, 2001).
[35] S. N. Majumdar, A. Rosso, and A. Zoia, Hitting probability for anomalous diffusion processes, Phys. Rev. Lett. **104**, 020602 (2010).
[36] M. Guéneau and L. Touzo, Relating absorbing and hard wall boundary conditions for a one-dimensional run-and-tumble particle, J. Phys. A **57**, 225005 (2024).
[37] P. Le Doussal, S. N. Majumdar, and G. Schehr, Velocity and diffusion constant of an active particle in a one-dimensional force field, Europhys. Lett. **130**, 40002 (2020).
[38] A. G. Cherstvy and R. Metzler, Ergodicity breaking and particle spreading in noisy heterogeneous diffusion processes, J. Chem. Phys. **142**, 144105 (2015).

[39] R. Metzler, J.-H. Jeon, A. G. Cherstvy, and E. Barkai, Anomalous diffusion models and their properties: Non-stationarity, non-ergodicity, and ageing at the centenary of single particle tracking, Phys. Chem. Chem. Phys. **16**, 24128 (2014).

[40] A. G. Cherstvy, A. V. Chechkin, and R. Metzler, Anomalous diffusion and ergodicity breaking in heterogeneous diffusion processes, New J. Phys. **15**, 083039 (2013).

[41] L. Garca-Coln, L. Del Castillo, and P. Goldstein, Theoretical basis for the Vogel-Fulcher-Tammann equation, Phys. Rev. B **40**, 7040 (1989).

[42] D. Martin, J. O'Byrne, M. E. Cates, É. Fodor, C. Nardini, J. Tailleur, and F. Van Wijland, Statistical mechanics of active Ornstein-Uhlenbeck particles, Phys. Rev. E **103**, 032607 (2021).

[43] A. J. Bray and A. J. McKane, Instanton calculation of the escape rate for activation over a potential barrier driven by colored noise, Phys. Rev. Lett. **62**, 493 (1989).

[44] L. Touzo and P. L. Doussal, Nonuniqueness of the steady state for run-and-tumble particles with a double-well interaction potential, Phys. Rev. E **113** 024106 (2026).